

Adaptive Resonance Theory-based Topological Clustering with a Divisive Hierarchical Structure Capable of Continual Learning

NAOKI MASUYAMA¹, (Member, IEEE), NARITO AMAKO¹, YUNA YAMADA¹, YUSUKE NOJIMA¹, (Member, IEEE), and HISAO ISHIBUCHI², (Fellow, IEEE).

¹Graduate School of Engineering, Osaka Prefecture University, 1-1 Gakuen-cho Naka-ku, Sakai-Shi, Osaka 599-8531, Japan (e-mails: {masuyama@narito.amako@ci., yuna.yamada@ci., nojima@jcs.osakafu-u.ac.jp})

²Guangdong Provincial Key Laboratory of Brain-inspired Intelligent Computation, Department of Computer Science and Engineering, Southern University of Science and Technology, Shenzhen 518055, China (e-mail: hisao@sustech.edu.cn)

Corresponding author: Hisao Ishibuchi (e-mail: hisao@sustech.edu.cn).

This research was supported by Ministry of Education, Culture, Sports, Science and Technology - JAPAN (MEXT) Leading Initiative for Excellent Young Researchers (LEADER), National Natural Science Foundation of China (Grant No. 61876075), Guangdong Provincial Key Laboratory (Grant No. 2020B121201001), the Program for Guangdong Introducing Innovative and Entrepreneurial Teams (Grant No. 2017ZT07X386), The Stable Support Plan Program of Shenzhen Natural Science Fund (Grant No. 20200925174447003), Shenzhen Science and Technology Program (Grant No. KQTD2016112514355531)

ABSTRACT Thanks to an ability for handling the plasticity-stability dilemma, Adaptive Resonance Theory (ART) is considered as an effective approach for realizing continual learning. In general, however, the clustering performance of ART-based algorithms strongly depends on a similarity threshold, i.e., a vigilance parameter, which is data-dependent and specified by hand. This paper proposes an ART-based topological clustering algorithm with a mechanism that automatically estimates a similarity threshold from a distribution of data points. In addition, for the improving information extraction performance, a divisive hierarchical clustering algorithm capable of continual learning is proposed by introducing a hierarchical structure to the proposed algorithm. Simulation experiments show that the proposed algorithm shows the comparative clustering performance compared with recently proposed hierarchical clustering algorithms.

INDEX TERMS Adaptive Resonance Theory, Topological Clustering, Hierarchical Clustering, Continual Learning.

I. INTRODUCTION

CLUSTERING is an essential technique to extract information from data. With the recent development of IoT technology, the significance of clustering increases as the availability of big data increases. Generally speaking, big data includes a wide range of useful information, e.g., hidden features of data and explicit/implicit relationships among data points and/or attributes. To utilize useful information in big data with a pluralistic and appropriate information granularity, information extraction approaches such as hierarchical clustering are widely studied. In particular, since a divisive hierarchical clustering algorithm can adaptively generate partitions in response to the changes in the data distribution, it has the potential to realize continual learning, which is an essential ability to efficiently utilize big data.

Typical divisive hierarchical clustering algorithms with an adaptive cluster structure are Growing Hierarchical Self-Organizing Map (GHSOM) [1] and Growing Hierarchical Neural Gas (GHNG) [2]. GHSOM applies Self-Organizing Map (SOM) [3] while GHNG applies Growing Neural Gas (GNG) [4] as a base clustering approach, which can grow in the vertical and horizontal directions by constructing a tree-like structure based on distributions of data points. However, in general, SOM-based and GNG-based clustering algorithms cannot avoid the plasticity-stability dilemma [5], i.e., the trade-off between catastrophic forgetting and continual learning of new information.

In the research field of clustering, Adaptive Resonance Theory (ART) [6] is a successful approach for handling the plasticity-stability dilemma. Since there are several ART-

based clustering algorithms have been proposed [7]–[12], Fast Topological Correntropy-Induced Metric-based ART (FTCA) [12] has superior clustering performance and functionality than others. FTCA utilizes the Correntropy-Induced Metric (CIM) [13] as a similarity measure for realizing a fast and stable self-organizing ability while maintaining an appropriate number of nodes. During a learning process, FTCA adaptively generates topological structures by using nodes and edges to efficiently extract information from a dataset.

In our previous study which is inspired by GHNG, we have introduced Hierarchical FTCA (HFTCA) to improve the clustering performance [14]. Although HFTCA showed the superior clustering performance than GHSOM and GHNG, HFTCA has a parameter (i.e., a similarity threshold) that significantly affects the clustering performance. In general, the optimal value of the similarity threshold depends on a dataset, which is a common difficulty in the use of ART-based clustering algorithms. Moreover, if an ART-based clustering algorithm has a hierarchical structure, it is necessary to specify a similarity threshold at each layer in advance. In this paper, to solve the above difficulty, we propose CIM-based ART with Edge and Age (CAEA), which introduces a mechanism to automatically estimate the similarity threshold from the distribution of data points. In addition, we also propose Hierarchical CAEA (HCAEA) for improving the clustering performance. Thanks to the continual learning ability of CAEA, HCAEA is also capable of continual learning.

The contributions of this paper are summarized as follows:

- (i) A new ART-based clustering algorithm, called CAEA, is proposed by introducing a mechanism to automatically estimate a similarity threshold from the distribution of data points.
- (ii) A new divisive hierarchical clustering algorithm, called HCAEA, is proposed by integrating CAEA and a hierarchical structure inspired by HFTCA.
- (iii) Empirical studies show that HCAEA has the comparative clustering performance than recently proposed hierarchical algorithms.

The paper is organized as follows. Section II presents the literature review for clustering algorithms and divisive hierarchical clustering algorithms. Section III describes details of the proposed algorithm and its hierarchical approach. Section IV presents simulation experiments to evaluate the information extraction ability by using real-world datasets. Section V summarizes characteristics of algorithms based on the experimental results. Section VI concludes this paper.

II. LITERATURE REVIEW

A. CLUSTERING ALGORITHMS CAPABLE OF CONTINUAL LEARNING

Clustering is one of the most widely used approaches for extracting information from data. Gaussian Mixture Model (GMM) [15] and k -means [16] are typical types of clustering algorithms. Although GMM and k -means are quite simple

and highly applicable, the number of classes needs to be specified in advance.

One effective approach for solving the drawback of GMM and k -means is a growing self-organizing clustering algorithm such as GNG [4] and Self-Organizing Incremental Neural Network (SOINN) [17]. GNG and SOINN can adaptively generate topological networks based on a distribution of data points. However, since these algorithms permanently insert new nodes into their networks for memorizing new information, they have the potential to forget learned information (i.e., catastrophic forgetting). This trade-off is called the plasticity-stability dilemma [5].

There are several clustering algorithms are proposed to cope with the plasticity-stability dilemma. As a GNG-based algorithm, Grow When Required (GWR) [18] and gamma-GWR [19] are successful algorithms which appropriately calculate a similarity threshold to prevent an excessive node creation. As a SOINN-based algorithm, SOINN+ [20] and SOINN+ with ghost nodes (GSOINN+) [21] can detect clusters of arbitrary shapes in noisy data streams while avoiding catastrophic forgetting. The other successful approach is ART-based clustering algorithms such as Fuzzy ART [7], Bayes ART [8], and their variants [9], [10]. In general, an ART-based clustering algorithm shows the superior clustering performance than GNG-based and SOINN-based algorithms [11], [12]. Moreover, because ART-based clustering algorithms theoretically realize sequential and class-incremental learning without catastrophic forgetting, a number of ART-based clustering algorithms and their improvements are proposed in both supervised learning [22]–[24] and unsupervised learning [7], [8], [25], [26]. One common drawback of ART-based clustering algorithms is a specification of a similarity threshold (i.e., a vigilance parameter). In most cases, the similarity threshold has a significant impact on the clustering performance while its optimal value of the similarity threshold depends on a dataset.

B. DIVISIVE HIERARCHICAL CLUSTERING ALGORITHMS

There are two types of hierarchical approaches, i.e., an agglomerative approach and a divisive approach [27]. An agglomerative hierarchical clustering algorithm takes a bottom-up approach that each data point is considered as separate clusters, and then merging them into a single cluster based on a similarity of clusters. A divisive hierarchical clustering algorithm takes a top-down approach that each data point is considered as a single cluster, and then dividing it into several different clusters based on dissimilarity of the clusters. In general, an agglomerative hierarchical clustering algorithm requires the entire dataset because of its learning procedure. In contrast, a divisive hierarchical clustering algorithm can be trained continually by adapting a cluster structure along with the changes in distributions of data points. Thanks to the above feature, a divisive hierarchical clustering algorithm has the potential to realize continual learning.

Typical divisive hierarchical clustering algorithms are the

bisecting k -means algorithm [28] and the principal direction divisive partitioning algorithm [29]. These algorithms are quite simple but show good clustering performance. However, these algorithms are not suitable for continual learning because they require all the training data to be given at once.

In order to realize a divisive hierarchical clustering algorithm capable of continuous learning, it is necessary to have abilities that adaptively extract information and build a hierarchical structure in response to given data. GHSOM [1] utilizes a growing SOM which can grow in the vertical and horizontal directions based on data distributions. One drawback of GHSOM is raised by a SOM architecture, that is, representing multiple data distributions in a single SOM network. Although the number of parameters is large, GHNG [2] has successfully solved the drawback of GHSOM by using GNG instead of SOM. Growing Hierarchical EXcitatory+INhibitory (GH-EXIN) [30] requires only a few parameters while maintaining a comparative performance to GHNG. In general, however, GNG-based clustering algorithms suffer from an excessive node creation and sensitivity to the presentation order of input data points. Moreover, the plasticity-stability dilemma [5], i.e., the trade-off between catastrophic forgetting and continual learning of new information, is another unavoidable problem. Applying an ART-based clustering algorithm as a basis of divisive hierarchical clustering is a promising approach because it can theoretically avoid the plasticity-stability dilemma. HFTCA [14] showed the superior clustering performance compared to GHSOM, GHNG, and GH-EXIN while maintaining a high information compression ratio. Although HFTCA is the state-of-the-art of ART-based divisive hierarchical clustering algorithm, HFTCA requires careful parameterization at each hierarchy in order to maintain good clustering performance.

III. PROPOSED ALGORITHM

In this section, first the theoretical background of the CIM is briefly described. Next, the proposed algorithm, namely,

CAEA, is explained in detail. Then, a hierarchical approach of HCAEA is introduced. Table 1 summarizes the main notations used in this paper.

A. CORRENTROPY AND CORRENTROPY-INDUCED METRIC

Correntropy [13] provides a generalized similarity measure between two arbitrary data points $\mathbf{x} = (x_1, x_2, \dots, x_d)$ and $\mathbf{y} = (y_1, y_2, \dots, y_d)$ as follows:

$$C(\mathbf{x}, \mathbf{y}) = E[\kappa_\sigma(\mathbf{x} - \mathbf{y})], \quad (1)$$

where $E[\cdot]$ is the expectation operation, and $\kappa_\sigma(\cdot)$ denotes a positive definite kernel with a kernel bandwidth σ . The correntropy can be estimated as follows:

$$\hat{C}(\mathbf{x}, \mathbf{y}) = \frac{1}{d} \sum_{i=1}^d \kappa_\sigma(x_i - y_i). \quad (2)$$

In this paper, we use the following Gaussian kernel in the correntropy:

$$\kappa_\sigma(x_i - y_i) = \exp\left[-\frac{(x_i - y_i)^2}{2\sigma^2}\right]. \quad (3)$$

A nonlinear metric called CIM is derived from the correntropy [13]. The CIM quantifies the similarity between two data points as follows:

$$\text{CIM}(\mathbf{x}, \mathbf{y}, \sigma) = \left[\kappa_\sigma(0) - \hat{C}(\mathbf{x}, \mathbf{y})\right]^{\frac{1}{2}}, \quad (4)$$

where $\kappa_\sigma(0) = 1$ from (3). Here, thanks to the Gaussian kernel without a coefficient $\frac{1}{\sqrt{2\pi}\sigma}$ as defined in (3), a range of the CIM is limited to $[0, 1]$.

In general, the Euclidean distance suffers from the curse of dimensionality while the CIM reduces the effect on it thanks to the correntropy which calculates a similarity between two arbitrary data points by using a kernel function. Moreover, it has also been shown that the CIM with the Gaussian kernel has a high outlier rejection capability [13].

TABLE 1: Summary of notations

Notation	Description
$X = \{\mathbf{x}_1, \mathbf{x}_2, \dots, \mathbf{x}_n, \dots\}$	A set of training data points
$\mathbf{x}_n = (x_{n,1}, x_{n,2}, \dots, x_{n,d})$	d -dimensional training data point (the n th data point)
$Y = \{\mathbf{y}_1, \mathbf{y}_2, \dots, \mathbf{y}_K\}$	A set of prototype nodes
$\mathbf{y}_k = (y_{k,1}, y_{k,2}, \dots, y_{k,d})$	d -dimensional prototype node (the k th node)
$S = \{\sigma_1, \sigma_2, \dots, \sigma_K\}$	A set of bandwidths for a kernel function
κ_σ	Kernel function with a bandwidth σ
CIM	Correntropy-Induced Metric
k_1, k_2	Indexes of the 1st and 2nd winner nodes
$\mathbf{y}_{k_1}, \mathbf{y}_{k_2}$	The 1st and 2nd winner nodes
V_{k_1}, V_{k_2}	Similarities between a data point \mathbf{x}_n and winner nodes (\mathbf{y}_{k_1} and \mathbf{y}_{k_2})
$V_{\text{threshold}}$	Similarity threshold (a vigilance parameter)
\mathcal{N}_{k_1}	A set of neighbor nodes of node \mathbf{y}_{k_1}
M_{k_1}	The number of data points that have accumulated by the node \mathbf{y}_{k_1}
λ	Predefined interval for computing σ and deleting an isolated node
$a_{(k_1, k_2)}$	Age of edge between nodes \mathbf{y}_{k_1} and \mathbf{y}_{k_2}
a_{max}	Predefined threshold of an age of edge
$e_{(k_1, k_2)}$	Edge connection between nodes \mathbf{y}_{k_1} and \mathbf{y}_{k_2}
$\mathbf{C} = (\mathbf{c}_1, \mathbf{c}_2, \dots, \mathbf{c}_K)$	Models of CAEA for constructing a hierarchical structure.

B. CIM-BASED ART WITH EDGE AND AGE

We use the following notations: A set of training data points are $X = \{\mathbf{x}_1, \mathbf{x}_2, \dots, \mathbf{x}_n, \dots\}$ where $\mathbf{x}_n = (x_{n,1}, x_{n,2}, \dots, x_{n,d})$ is a d -dimensional feature vector. A set of prototype nodes in CAEA at the point of the presentation of a data point \mathbf{x}_n is $Y = \{\mathbf{y}_1, \mathbf{y}_2, \dots, \mathbf{y}_K\}$ ($K \in \mathbb{Z}^+$) where a node $\mathbf{y}_k = (y_1, y_2, \dots, y_d)$ has the same dimension as \mathbf{x}_n . Furthermore, each node \mathbf{y}_k has an individual bandwidth σ for the CIM, i.e., $S = \{\sigma_1, \sigma_2, \dots, \sigma_K\}$.

The learning procedure of CAEA is divided into five parts: 1) initialization process for nodes and a bandwidth of a kernel function in the CIM, 2) winner node selection, 3) vigilance test, and 4) node learning and edge construction. Each of them is explained in the following subsections.

1) Initialization Process for Nodes and a Bandwidth of a Kernel Function in the CIM

In the case that CAEA does not have any nodes, i.e., a set of prototype node $\mathcal{Y} = \emptyset$, the 1st to $\lambda/2$ th training data points $X_{\text{init}} = \{\mathbf{x}_1, \mathbf{x}_2, \dots, \mathbf{x}_{\lambda/2}\}$ directly become prototype nodes, i.e., $Y_{\text{init}} = \{\mathbf{y}_1, \mathbf{y}_2, \dots, \mathbf{y}_{\lambda/2}\}$, where $\lambda \in \mathbb{Z}^+$ is a predefined parameter of CAEA. This parameter is also used for a node deletion process.

In an ART-based clustering algorithm, a vigilance parameter (i.e., a similarity threshold) plays an important role in a self-organizing process. Typically, the similarity threshold is data-dependent and specified by hand. On the other hand, CAEA uses the minimum pairwise CIM value between each of nodes in $Y_{\text{init}} = \{\mathbf{y}_1, \mathbf{y}_2, \dots, \mathbf{y}_{\lambda/2}\}$, and the average of pairwise CIM values is used as the similarity threshold $V_{\text{threshold}}$, i.e.,

$$V_{\text{threshold}} = \frac{1}{\lambda/2} \sum_{i=1}^{\lambda/2} \min_{j \neq i} [\text{CIM}(\mathbf{y}_i, \mathbf{y}_j, \sigma)], \quad (5)$$

where σ is a kernel bandwidth in the CIM.

In general, a bandwidth of a kernel function σ can be estimated based on a kernel density estimator [31], which is defined as follows:

$$\Sigma = U(F_\nu) \Gamma N^{-\frac{1}{2\nu+d}}, \quad (6)$$

$$U(F_\nu) = \left(\frac{\pi^{d/2} 2^{d+\nu-1} (\nu!)^2 R(F)^d}{\nu \kappa_\nu^2(F) [(2\nu)!! + (d-1)(\nu!!)^2]} \right)^{\frac{1}{2\nu+d}}, \quad (7)$$

where Γ denotes a rescale operator (d -dimensional vector) which is defined by a standard deviation of the d attributes among N training data points. ν is the order of a kernel. $R(F)$ is a roughness function. $\kappa_\nu(F)$ is the moment of a kernel. The details of the derivation of (6) can be found in [31].

In this paper, we set $N = \lambda/2$, and we utilize the Gaussian kernel for the CIM. Therefore, $\nu = 2$, $R(F) = (2\sqrt{\pi})^{-1}$, and $\kappa_\nu^2(F) = 1$ are derived. As a result, we obtain:

$$\Sigma = \left(\frac{4}{2+d} \right)^{\frac{1}{4+d}} \Gamma (\lambda/2)^{-\frac{1}{4+d}}. \quad (8)$$

Here, Σ contains the bandwidth of each attribute. In this paper, the median of Σ is selected as a representative bandwidth of the Gaussian kernel in the CIM, i.e.,

$$\sigma = \text{median}(\Sigma). \quad (9)$$

In CAEA, the initial prototype nodes $Y_{\text{init}} = \{\mathbf{y}_1, \mathbf{y}_2, \dots, \mathbf{y}_{\lambda/2}\}$ have a common bandwidth of the Gaussian kernel in the CIM, i.e., $S_{\text{init}} = \{\sigma_1, \sigma_2, \dots, \sigma_{\lambda/2}\}$. When a new node $\mathbf{y}_{(\lambda/2)+1}$ is generated from $\mathbf{x}_{(\lambda/2)+1}$, a bandwidth $\sigma_{(\lambda/2)+1}$ is estimated from the past $\lambda/2$ data points, i.e., $\{\mathbf{x}_{n-\lambda/2}, \dots, \mathbf{x}_{n-2}, \mathbf{x}_{n-1}\}$, by using (6) and (7). As a result, each new node has a different bandwidth σ depending on distributions of training data points. Although the similarity threshold $V_{\text{threshold}}$ depends on a distribution of the initial $\lambda/2$ training data points, we regard that an adaptive $V_{\text{threshold}}$ estimation is realized by assigning a different bandwidth σ , which affects the CIM value, for each node in response to the changes in the data distribution.

2) Winner Node Selection

Once a data point \mathbf{x}_n is presented to CAEA, two nodes which have a similar state to the data point \mathbf{x}_n are selected, namely, winner nodes \mathbf{y}_{k_1} and \mathbf{y}_{k_2} . The winner nodes are determined based on the state of the CIM as follows:

$$k_1 = \arg \min_{\mathbf{y}_i \in \mathcal{Y}} [\text{CIM}(\mathbf{x}_n, \mathbf{y}_i, \text{mean}(S))], \quad (10)$$

$$k_2 = \arg \min_{\mathbf{y}_i \in \mathcal{Y} \setminus \{\mathbf{y}_{k_1}\}} [\text{CIM}(\mathbf{x}_n, \mathbf{y}_i, \text{mean}(S))], \quad (11)$$

where k_1 and k_2 denote indexes of the 1st and 2nd winner nodes i.e., \mathbf{y}_{k_1} and \mathbf{y}_{k_2} , respectively. S is a bandwidth of the Gaussian kernel in the CIM for each node.

3) Vigilance Test

Similarities between a data point \mathbf{x}_n and the 1st and 2nd winner nodes are defined as follows:

$$V_{k_1} = \text{CIM}(\mathbf{x}_n, \mathbf{y}_{k_1}, \text{mean}(S)), \quad (12)$$

$$V_{k_2} = \text{CIM}(\mathbf{x}_n, \mathbf{y}_{k_2}, \text{mean}(S)). \quad (13)$$

The vigilance test classifies the relationship between a data point and a node into three cases by using a predefined similarity threshold $V_{\text{threshold}}$, i.e.,

- Case I

A similarity between a data point \mathbf{x}_n and the 1st winner node \mathbf{y}_{k_1} is larger (i.e., less similar) than $V_{\text{threshold}}$, namely:

$$V_{k_1} > V_{\text{threshold}}. \quad (14)$$

If (14) is satisfied, $V_{k_2} > V_{\text{threshold}}$ is also satisfied since $V_{k_2} > V_{k_1} > V_{\text{threshold}}$.

- Case II

A similarity between a data point \mathbf{x}_n and the 1st winner node \mathbf{y}_{k_1} is smaller (i.e., more similar) than $V_{\text{threshold}}$, and a

similarity between the data point \mathbf{x}_n and the 2nd winner node \mathbf{y}_{k_2} is larger (i.e., less similar) than $V_{\text{threshold}}$, namely:

$$V_{k_1} \leq V_{\text{threshold}} \wedge V_{k_2} > V_{\text{threshold}}. \quad (15)$$

• Case III

Similarities between a data point \mathbf{x}_n and the 1st and 2nd winner nodes are both smaller (i.e., more similar) than $V_{\text{threshold}}$, namely:

$$V_{k_1} \leq V_{\text{threshold}} \wedge V_{k_2} \leq V_{\text{threshold}}. \quad (16)$$

4) Node Learning and Edge Construction

Depending on the result of the vigilance test, a different operation is performed.

If \mathbf{x}_n is classified as Case I by the vigilance test (i.e., (14) is satisfied), a new node is defined as $\mathbf{y}_{K+1} = \mathbf{x}_n$. A bandwidth σ_{K+1} for node \mathbf{y}_{K+1} is calculated by (9). In addition, the number of data points that have been accumulated by the node \mathbf{y}_{K+1} is initialized as $M_{K+1} = 1$.

If \mathbf{x}_n is classified as Case II by the vigilance test (i.e., (15) is satisfied), first, an age of the edge connected to node \mathbf{y}_{k_1} is updated as follows:

$$a_{(k_1,j)} \leftarrow a_{(k_1,j)} + 1 \quad (\forall j \in \mathcal{N}_{k_1}), \quad (17)$$

where \mathcal{N}_{k_1} is a set of neighbor nodes of \mathbf{y}_{k_1} . After updating the age of edge, an edge whose age is greater than a predefined threshold a_{max} is deleted. Then, the node \mathbf{y}_{k_1} is updated as follows:

$$\mathbf{y}_{k_1} \leftarrow \mathbf{y}_{k_1} + \frac{1}{M_{k_1}} (\mathbf{x}_n - \mathbf{y}_{k_1}). \quad (18)$$

When updating the node, the amount of change is divided by M_{k_1} , so the larger M_{k_1} becomes, the smaller the node position changes. This is based on the idea that the information around a node, where data points are frequently given, is important and should be held by the node.

In Case II, a counter M for the number of data points that have been accumulated by the node \mathbf{y}_{k_1} is also updated as follows:

$$M_{k_1} \leftarrow M_{k_1} + 1. \quad (19)$$

If \mathbf{x}_n is classified as Case III by the vigilance test (i.e., (16) is satisfied), the same operations as Case II (i.e., (17), (18), and (19)) are performed. In addition, the neighbor nodes of \mathbf{y}_{k_1} are updated as follows:

$$\mathbf{y}_j \leftarrow \mathbf{y}_j + \frac{1}{10M_j} (\mathbf{x}_n - \mathbf{y}_j) \quad (\forall j \in \mathcal{N}_{k_1}). \quad (20)$$

Equation (20) has the same concept as (18), but it should be less affected by the data point than \mathbf{y}_{k_1} because it is the neighbor node of \mathbf{y}_{k_1} . Thus, the value is multiplied by 1/10.

If there is no edge between nodes \mathbf{y}_{k_1} and \mathbf{y}_{k_2} , a new edge is generated and an age of the edge is initialized as follows:

$$a_{(k_1,k_2)} \leftarrow 0. \quad (21)$$

In the case that there is an edge between nodes \mathbf{y}_{k_1} and \mathbf{y}_{k_2} , then an age of the edge is reset as (21).

Apart from the above operations in Cases I-III, as a noise reduction purpose, the nodes without edges are deleted every time λ training data points are given.

The learning procedure of CAEA is summarized in Algorithm 1.

Algorithm 1: Learning Algorithm of CAEA

Input:

a set of training data points: $X = \{\mathbf{x}_1, \mathbf{x}_2, \dots, \mathbf{x}_n, \dots\}$

where $\mathbf{x}_n = (x_{n,1}, x_{n,2}, \dots, x_{n,d})$ ($\mathbf{x}_l \in \mathbb{R}^d$),

the interval for computing σ and deleting an isolated node:

λ ,

and the threshold of an age of edge: a_{max} .

Output:

the CAEA model.

model contents

a set of generated nodes: $Y = \{\mathbf{y}_1, \mathbf{y}_2, \dots, \mathbf{y}_K\}$
($K \in \mathbb{Z}^+$),

a set of bandwidths for a kernel function:

$S = \{\sigma_1, \sigma_2, \dots, \sigma_K\}$

a set of counters: $M = \{M_1, M_2, \dots, M_K\}$,

the matrix of edge connections: \mathbf{e} ,

and the matrix of edge age: \mathbf{a} .

```

1 function LearningCAEA(X, λ, e_max)
2   forall l ∈ 1, 2, ..., L do
3     if K < λ/2 then
4       Create the new node as y_{K+1} = x_l.
5       Calculate the kernel bandwidth σ_{K+1} by (8)
        and (9).
6       if K = λ/2 then
7         Calculate the vigilance parameter V_{threshold}
          by (5).
8     else
9       Search the indexes of winner nodes k_1 and k_2
        by (10) and (11), respectively.
10      Update the edge age a_{(k_1,j)} by (17).
11      if e_{(k_1,j)} > e_max then
12        Delete the edge.
13      if V_{k_1} > V_{threshold} then
14        Create the new node as y_{K+1} = x_l.
15        Calculate the kernel bandwidth σ_{k+1} by
          (8) and (9).
16      else
17        Update the state of y_{k_1} by (18).
18        if V_{k_2} ≤ V_{threshold} then
19          Update the state of neighbor nodes y_j
            by (20).
20          Create a new edge e_{(k_1,k_2)} between
            y_{k_1} and y_{k_2}.
21      if the number of data point inputs l is multiple of a
        topology adjustment cycle λ then
22        forall k ∈ 1, 2, ..., K do
23          if y_k does not have any edge then
24            Remove y_k from Y.
25  return the CAEA model.
```

C. HIERARCHICAL APPROACH FOR CAEA

The procedure for creating the hierarchical structure of HCAEA is as follows: First, CAEA is trained with a set

of training data points $X = \{\mathbf{x}_1, \mathbf{x}_2, \dots, \mathbf{x}_n, \dots\}$ to generate a topological network (nodes and edges) in the first layer, then supposing $Y = \{\mathbf{y}_1, \mathbf{y}_2, \dots, \mathbf{y}_K\}$ is generated. Here, we preserve training data points that affect to a node y_k during training process. As a result, we define a new set of K training data point set $X' = \{X_1, X_2, \dots, X_K\}$ ($X' \in X$) for the second layer. In the second layer, CAEA is independently trained by using the subset of training data points X_k . As a general description, CAEA in the $(h+1)$ th layer is independently trained by using the subset of training data points defined by the nodes in the h th layer. The above procedure is repeated until a topological network is no longer organized by CAEA. That is, when the number of nodes K becomes two in the h th layer, it is too small to represent a distribution of data. As a result, the training in the $(h+1)$ th layer is stopped.

The learning procedure of HCAEA is summarized in Algorithm 2.

Algorithm 2: Learning Algorithm of HCAEA

Input:

a set of training data points: $X = \{\mathbf{x}_1, \mathbf{x}_2, \dots, \mathbf{x}_n, \dots\}$
 where $\mathbf{x}_n = (x_{n,1}, x_{n,2}, \dots, x_{n,d})$ ($\mathbf{x}_l \in \mathbb{R}^d$),
 the interval for computing σ and deleting an isolated node:
 λ ,
 and the threshold of an age of edge: a_{\max} .

Output:

the HCAEA model.

model contents

a set of training data points for the next layer: $X' = \{X_1, X_2, \dots, X_K\}$ ($X' \in X$),
 a set of generated nodes:
 $Y = \{\mathbf{y}_1, \mathbf{y}_2, \dots, \mathbf{y}_K\}$ ($K \in \mathbb{Z}^+$),
 a set of bandwidths for a kernel function:
 $S = \{\sigma_1, \sigma_2, \dots, \sigma_K\}$
 a set of counters: $M = \{M_1, M_2, \dots, M_K\}$,
 the matrix of edge connections: \mathbf{e} ,
 the matrix of age of edge: \mathbf{a} ,
 and a set of child models: $C = \{\mathbf{c}_1, \mathbf{c}_2, \dots, \mathbf{c}_K\}$.

```

1 function LearningHCAEA( $X, \lambda, a_{\max}$ )
2   HCAEA model = LearningCAEA( $\mathbf{X}, \lambda, a_{\max}$ ).
3   if  $K \geq 2$  then
4     forall  $k \in 1, 2, \dots, K$  do
5       Extract a set of data points  $X_k$  that have
        accumulated by the node  $y_k$  as the training
        data points for the next layer.
6        $\mathbf{c}_k = \text{LearningHCAEA}(X_k, \lambda, a_{\max})$ .
7     Update the HCAEA model.
8   else
9     return.
10  return the HCAEA model.
  
```

IV. SIMULATION EXPERIMENTS

In this section, we compare the clustering performance of CAEA, HCAEA, GHNG [2], GH-EXIN [30], and HFTCA [14] based on the classification performance. In general, the evaluation of the clustering performance is subjective if a dataset does not have label information (i.e., the number

of classes in the dataset is not specified). In this paper, therefore, we use datasets with label information and perform classification tasks by using a clustering result as a classifier. This approach allows us to indirectly evaluate the clustering performance, that is, the performance of approximating the data distribution.

The source code of GHNG ¹, GH-EXIN ², and HFTCA ³ are provided by authors.

A. DATASETS

We utilize five synthetic datasets and nine real-world datasets selected from the commonly used clustering benchmarks [32] and public repositories [33], [34]. Table 2 summarizes statistics of the datasets.

TABLE 2: Statistics of datasets for classification tasks

Type	Dataset	Number of Attributes	Number of Classes	Number of Instances
Synthetic	Aggregation	2	7	788
	Compound	2	6	299
	Hard Distribution	2	3	1,500
	Jain	2	2	373
	Pathbased	2	3	300
Real-world	COIL20	1,024	20	1,440
	Iris	4	3	150
	Isolet	617	26	1,560
	OptDigits	64	10	5,620
	Seeds	7	3	210
	Semeion	256	10	1,593
	Sonar	60	2	208
	TOX171	5,748	4	171
	Wine	13	3	178

B. PARAMETER SPECIFICATIONS

CAEA, HCAEA, GHNG [2], GH-EXIN [30], and HFTCA [14] have parameters which have an impact on the clustering performance. This section presents parameter specifications of each algorithm in detail.

Table 3 summarizes parameter settings of each algorithm. In each algorithm, one parameter which has a large impact on the clustering performance is specified by grid search while the other parameters are specified as follows: In GHNG, the most of parameters are the same as GNG. Therefore, we apply the commonly used GNG parameter settings. In GH-EXIN, some parameters are the same as GNG while \min_{card} and H_{perc} are unique ones. \min_{card} and H_{perc} are specified by referencing a provided code and [30]. In HFTCA, a vigilance parameter of each layer has to be determined in advance. A topology construction cycle λ is the same specification as used in [14].

During grid search in our experiment, the training data points in each dataset are presented to each algorithm only once without pre-processing. In addition, the training data

¹<http://www.lcc.uma.es/~ejpalomo/software.html>

²<https://github.com/pietrobarbiero/ghexin>

³<https://github.com/Masuyama-lab/HFTCA>

TABLE 3: Parameter settings of each algorithm for classification tasks

Algorithm	Parameter	Value	Grid Range	Description
GHNG	τ	grid search	{0.001, 0.01, 0.05, 0.1, 0.15, 0.2, 0.25, 0.3, 0.35, 0.4, 0.45, 0.5}	a learning coefficient
	ϵ_W	0.2	—	a learning coefficient
	ϵ_N	0.006	—	a learning coefficient
	α	0.5	—	a learning coefficient
	β	0.995	—	a learning coefficient
	age_{\max}	50	—	a maximum age of edge
	λ	100	—	a node insertion cycle
GH-EXIN	H_{\max}	grid search	{0.00001, 0.0001, 0.001, 0.01, 0.1, 0.2, 0.3, 0.4, 0.5, 0.6, 0.7, 0.8, 0.9, 1.0}	a task-dependent index
	min_{card}	100	—	a data cardinality
	H_{perc}	0.5	—	a stopping criterion
	ϵ_W	0.2	—	a learning coefficient
	ϵ_N	0.006	—	a learning coefficient
	age_{\max}	50	—	a maximum age of edge.
	λ	100	—	a topology construction cycle
HFTCA	V_1, V_2, \dots, V_L	grid search	{0.05, 0.1, 0.2, 0.3, 0.4, 0.5, 0.6, 0.7, 0.8, 0.9, 0.95}	a vigilance parameter of each layer
	λ	100	—	a topology construction cycle
CAEA	λ	grid search	{10, 12, 14, 16, 18, 20, 22, 24, 26, 28, 30}	an interval for adapting σ
	a_{\max}	10	—	a maximum age of edge
HCAEA	λ	grid search	{10, 12, 14, 16, 18, 20, 22, 24, 26, 28, 30}	an interval for adapting σ
	a_{\max}	10	—	a maximum age of edge

TABLE 4: Parameters specified by grid search for classification tasks

Type	Dataset	GHNG	GH-EXIN	HFTCA	CAEA	HCAEA
		τ	H_{\max}	$(V_1, V_2, V_3, V_4, V_5)$	λ	λ
Synthetic	Aggregation	0.200	0.30000	(0.95, 0.95, 0.60, -, -)	30	30
	Compound	0.100	0.00010	(0.95, 0.95, 0.10, -, -)	26	30
	Hard Distribution	0.010	0.00001	(0.70, 0.40, 0.30, 0.20, 0.10)	26	28
	Jain	0.300	0.10000	(0.90, 0.90, 0.80, 0.30, -)	26	26
	Pathbased	0.001	0.01000	(0.90, 0.80, 0.70, -, -)	28	28
Real-world	Breast Cancer	0.300	0.00001	(0.70, 0.60, 0.20, -, -)	26	26
	COIL20	0.010	0.00001	(0.40, -, -, -, -)	26	26
	Iris	0.500	0.00001	(0.80, 0.70, 0.50, -, -)	28	28
	Ioslet	0.150	0.00100	(0.70, 0.60, -, -, -)	30	30
	OptDigits	0.001	0.40000	(0.70, -, -, -, -)	20	20
	Seeds	0.100	0.00010	(0.80, 0.60, 0.40, -, -)	28	16
	Sonar	0.250	0.00100	(0.40, -, -, -, -)	24	24
	TOX171	0.300	0.00100	N/A	26	26
	Wine	0.150	0.20000	(0.90, 0.80, 0.50, -, -)	24	28

N/A indicates that an algorithm could not build a predictive model.

A symbol "-" in HFTCA means that a layer is not generated.

point is input under a stationary environment, i.e., the training data points are randomly selected from the entire data. For each parameter specification, we repeat the evaluation 20 times (i.e., 2×10 -fold cross validation) with a different random seed for obtaining consistent averaging results.

Table 4 summarizes parameters which are specified by grid search. By applying the parameter specifications in Tables 3 and 4, each algorithm shows the highest Normalized Mutual Information (NMI) [35] score for each dataset under a stationary environment. Note that a symbol "-" in HFTCA means that the layer is not generated.

C. CLASSIFICATION TASKS

1) Conditions

In order to demonstrate the ability of continuous learning, we conduct classification tasks not only in the stationary environment but also the non-stationary environment. In the

stationary environment, the training data points are randomly selected from the entire dataset. In the non-stationary environment, the training data points are randomly selected from a specific class of a dataset, and the class is shifted sequentially.

During our experiments, the training data points in each dataset are presented to each algorithm only once with no pre-processing. We repeat the evaluation 20 times (i.e., 2×10 -fold cross validation) with a different random seed for obtaining consistent averaging results. The parameters of each algorithm are specified as in Table 3 for both in stationary and non-stationary environments. The classification performance is evaluated by Accuracy, NMI [35], Adjusted Rand Index (ARI) [36], and macro- F_1 .

As a statistical analysis, the Friedman test and Nemenyi post-hoc analysis [37] are utilized. The Friedman test is used to test the null hypothesis that all algorithms perform equally.

If the null hypothesis is rejected, the Nemenyi post-hoc analysis is then conducted. The Nemenyi post-hoc analysis is used for all pairwise comparisons based on the ranks of results over all the evaluation metrics of all datasets. Here, the null hypothesis is rejected at the significance level of 0.05 both in the Friedman test and the Nemenyi post-hoc analysis. All computations are carried out on Matlab 2020a with 2.2GHz Xeon Gold 6238R processor and 768GB RAM.

2) Stationary Environment

Table 5 shows the results of the classification performance in the stationary environment. The best value in each metric is indicated by bold. The standard deviation is indicated in parentheses. N/A indicates that an algorithm could not build a predictive model. As an overall trend, GH-EXIN and HCAEA show the better performance than CAEA, GHNG and HFTCA. Here, the null hypothesis is rejected on the Friedman test over all the evaluation metrics and datasets thus we apply the Nemenyi post-hoc analysis. Fig. 1 shows a critical difference diagram based on the classification performance including all the evaluation metrics and datasets. A better specification has lower average ranks, i.e., on the right side of a critical distance diagram. In theory, the parameter specifications within a critical distance (i.e., a red line) do not have a statistically significance difference [37]. In Fig. 1, GH-EXIN shows the best performance but there is no statistically significant difference between HCAEA. Comparing HCAEA and CAEA, although there is no statistically significant difference, HCAEA shows a lower rank. This suggests that a divisive hierarchical structure of HCAEA has a positive impact on the classification/clustering performance.

Table 6 shows the number of generated nodes by each algorithm in the stationary environment. As a general tendency, GH-EXIN generates a very large number of nodes and GHNG generates a very small number of nodes. The number of nodes in HCAEA is larger than that of CAEA because of a hierarchical structure. Note that the number of layers of HCAEA is automatically specified by the algorithm. In this experiment, HCAEA generates a single layer for COIL20, Isolet, Sonar, TOX171, and Wine datasets. These datasets tend to have a small number of training data points compared to the number of attributes. From the above observation, it can be regarded that HCAEA can adaptively and automatically specify the sufficient number of nodes and layers for extracting information.

Table 7 summarizes the results of training time on CPU in the stationary environment. In general, GHNG is faster than other algorithms because the number of generated nodes is smaller than others. Regarding GH-EXIN, the computation speed depends on the number of attributes in a dataset. Namely, GH-EXIN is fast when the number of attributes is small while it is slow when the number of attributes is large. In the case of HCAEA and CAEA, the computation speed is depending on the number of generated nodes. In short, the computation speed is slow when the number of generated nodes is large, and vice versa.

3) Non-stationary Environment

In the case of the non-stationary environment, a continual learning ability is required to maintain the classification/clustering performance because the training data points are randomly selected from a specific class of a dataset, and the class is shifted sequentially.

In general, whether an environment is stationary or non-stationary is unknown and dynamic. In other words, an algorithm should have characteristics that do not deteriorate its classification/clustering performance in any environment. For this reason, the parameter specifications in the non-stationary environment are the same as in the stationary environment, i.e., Tables 3 and 4.

Table 8 shows the results of the classification performance in the stationary environment. The best value in each metric is indicated by bold. The standard deviation is indicated in parentheses. N/A indicates that an algorithm could not build a predictive model. Similar to the stationary environment, the classification performance of GH-EXIN and HCAEA is generally better than CAEA, GHNG and HFTCA. Here, the null hypothesis is rejected on the Friedman test over all the evaluation metrics and datasets thus we apply the Nemenyi post-hoc analysis. Fig. 2 shows a critical difference diagram based on the classification performance including all the evaluation metrics and datasets. Similar to the result of the stationary environment, GH-EXIN shows the best performance but there is no statistically significant difference between HCAEA. Regarding HCAEA and CAEA, there is a statistically significant difference between the performance of those algorithms. This result indicates that HCAEA has the stable and superior information extraction ability than CAEA regardless of the stationary or non-stationary environments.

Table 9 shows the number of generated nodes by each algorithm in the non-stationary environment. The general trend is the same as in the stationary environment, where GH-EXIN has a large number of generated nodes and GHNG has a small one. Regarding HCAEA, the algorithm generates a single layer for COIL20, Isolet, Sonar, TOX171, and Wine datasets, which are the same as the stationary environment.

Table 10 summarizes the results of training time on CPU in the non-stationary environment. The general trend of the computation speed is also the same as the stationary environment. Namely, GHNG is faster, the computation speed of GH-EXIN depends on the number of attributes, and the computation speed of HCAEA and CAEA depends on the number of generated nodes.

V. DISCUSSION

This section summarizes the characteristics of each algorithm based on the experimental results in Sections IV-C2 and IV-C3 for emphasizing the advantages of HCAEA and CAEA.

In regard to GHNG, the computation speed is faster than other algorithms. However, the information extraction performance is inferior to others. One possible reason is that a network generated by GNG does not adequately approximate

TABLE 5: Results of the classification performance in the stationary environment

Type	Dataset	Metric	GHNG	GH-EXIN	HFTCA	CAEA	HCAEA
Synthetic	Aggregation	Accuracy	0.896 (0.048)	0.993 (0.009)	0.489 (0.059)	0.957 (0.051)	0.996 (0.006)
		NMI	0.883 (0.047)	0.987 (0.016)	0.337 (0.049)	0.948 (0.057)	0.992 (0.012)
		ARI	0.825 (0.074)	0.986 (0.018)	0.227 (0.063)	0.929 (0.077)	0.992 (0.013)
		macro-F ₁	0.701 (0.107)	0.987 (0.018)	0.300 (0.045)	0.872 (0.116)	0.992 (0.014)
	Compound	Accuracy	0.783 (0.107)	0.930 (0.042)	0.574 (0.072)	0.871 (0.055)	0.956 (0.030)
		NMI	0.796 (0.080)	0.906 (0.044)	0.443 (0.081)	0.861 (0.058)	0.936 (0.039)
		ARI	0.704 (0.146)	0.888 (0.070)	0.361 (0.122)	0.797 (0.088)	0.916 (0.062)
		macro-F ₁	0.589 (0.185)	0.911 (0.050)	0.329 (0.055)	0.794 (0.107)	0.945 (0.049)
	HardDistribution	Accuracy	0.989 (0.009)	0.995 (0.006)	0.992 (0.007)	0.987 (0.008)	0.984 (0.012)
		NMI	0.955 (0.031)	0.976 (0.025)	0.967 (0.030)	0.950 (0.029)	0.939 (0.039)
		ARI	0.968 (0.025)	0.984 (0.017)	0.976 (0.022)	0.962 (0.023)	0.953 (0.034)
		macro-F ₁	0.989 (0.009)	0.995 (0.005)	0.992 (0.007)	0.987 (0.008)	0.984 (0.012)
	Jain	Accuracy	0.887 (0.068)	1.000 (0.000)	0.842 (0.055)	0.991 (0.016)	0.999 (0.006)
		NMI	0.503 (0.224)	1.000 (0.000)	0.304 (0.156)	0.937 (0.103)	0.991 (0.039)
		ARI	0.569 (0.230)	1.000 (0.000)	0.417 (0.174)	0.959 (0.069)	0.994 (0.025)
		macro-F ₁	0.835 (0.107)	1.000 (0.000)	0.771 (0.087)	0.986 (0.023)	0.998 (0.007)
Pathbased	Accuracy	0.653 (0.095)	0.955 (0.038)	0.548 (0.101)	0.905 (0.071)	0.982 (0.025)	
	NMI	0.476 (0.109)	0.871 (0.105)	0.181 (0.094)	0.788 (0.114)	0.947 (0.071)	
	ARI	0.363 (0.137)	0.862 (0.113)	0.124 (0.098)	0.753 (0.156)	0.943 (0.080)	
	macro-F ₁	0.594 (0.105)	0.956 (0.039)	0.527 (0.105)	0.897 (0.074)	0.982 (0.024)	
Real-world	Breast Cancer	Accuracy	0.889 (0.057)	0.914 (0.033)	0.887 (0.044)	0.910 (0.039)	0.909 (0.041)
		NMI	0.541 (0.176)	0.588 (0.118)	0.503 (0.161)	0.588 (0.136)	0.586 (0.139)
		ARI	0.606 (0.172)	0.679 (0.110)	0.594 (0.141)	0.667 (0.132)	0.665 (0.135)
		macro-F ₁	0.878 (0.058)	0.904 (0.037)	0.875 (0.050)	0.900 (0.043)	0.900 (0.043)
	COIL20	Accuracy	0.433 (0.056)	0.830 (0.043)	0.705 (0.057)	0.555 (0.062)	0.555 (0.062)
		NMI	0.716 (0.037)	0.892 (0.027)	0.832 (0.023)	0.735 (0.035)	0.735 (0.035)
		ARI	0.416 (0.060)	0.765 (0.069)	0.627 (0.060)	0.446 (0.072)	0.446 (0.072)
		macro-F ₁	0.333 (0.049)	0.815 (0.045)	0.654 (0.056)	0.462 (0.068)	0.462 (0.068)
	Iris	Accuracy	0.883 (0.068)	0.960 (0.055)	0.947 (0.056)	0.967 (0.046)	0.960 (0.050)
		NMI	0.806 (0.070)	0.917 (0.111)	0.888 (0.099)	0.927 (0.096)	0.913 (0.106)
		ARI	0.747 (0.118)	0.896 (0.143)	0.873 (0.115)	0.909 (0.128)	0.895 (0.134)
		macro-F ₁	0.846 (0.112)	0.950 (0.075)	0.924 (0.100)	0.960 (0.061)	0.950 (0.067)
	Isolet	Accuracy	0.505 (0.078)	0.812 (0.014)	0.482 (0.031)	0.332 (0.032)	0.332 (0.032)
		NMI	0.681 (0.029)	0.828 (0.011)	0.613 (0.023)	0.515 (0.020)	0.515 (0.020)
		ARI	0.423 (0.044)	0.691 (0.021)	0.351 (0.026)	0.199 (0.024)	0.199 (0.024)
		macro-F ₁	0.465 (0.090)	0.808 (0.013)	0.444 (0.042)	0.274 (0.034)	0.274 (0.034)
	OptDigits	Accuracy	0.899 (0.016)	0.953 (0.010)	0.760 (0.021)	0.841 (0.085)	0.835 (0.112)
		NMI	0.832 (0.026)	0.912 (0.018)	0.637 (0.033)	0.766 (0.077)	0.757 (0.109)
		ARI	0.797 (0.031)	0.901 (0.022)	0.565 (0.042)	0.710 (0.114)	0.701 (0.162)
		macro-F ₁	0.898 (0.017)	0.953 (0.010)	0.753 (0.018)	0.832 (0.099)	0.826 (0.125)
	Seeds	Accuracy	0.881 (0.059)	0.843 (0.064)	0.864 (0.060)	0.869 (0.065)	0.876 (0.059)
		NMI	0.715 (0.123)	0.639 (0.132)	0.691 (0.117)	0.703 (0.136)	0.702 (0.113)
		ARI	0.669 (0.149)	0.596 (0.146)	0.654 (0.141)	0.650 (0.163)	0.665 (0.142)
		macro-F ₁	0.872 (0.064)	0.825 (0.074)	0.848 (0.070)	0.862 (0.067)	0.865 (0.060)
	Sonar	Accuracy	0.493 (0.115)	0.664 (0.099)	0.625 (0.089)	0.688 (0.116)	0.688 (0.116)
		NMI	0.038 (0.043)	0.149 (0.120)	0.083 (0.070)	0.182 (0.162)	0.182 (0.162)
		ARI	0.014 (0.034)	0.111 (0.117)	0.064 (0.076)	0.160 (0.162)	0.160 (0.162)
		macro-F ₁	0.453 (0.123)	0.651 (0.100)	0.614 (0.087)	0.674 (0.121)	0.674 (0.121)
TOX171	Accuracy	0.346 (0.119)	0.424 (0.086)	N/A	0.471 (0.139)	0.471 (0.139)	
	NMI	0.239 (0.138)	0.357 (0.110)	N/A	0.359 (0.126)	0.359 (0.126)	
	ARI	0.080 (0.069)	0.143 (0.137)	N/A	0.125 (0.113)	0.125 (0.113)	
	macro-F ₁	0.250 (0.098)	0.367 (0.092)	N/A	0.387 (0.136)	0.387 (0.136)	
Wine	Accuracy	0.657 (0.086)	0.657 (0.098)	0.874 (0.081)	0.876 (0.089)	0.846 (0.122)	
	NMI	0.475 (0.118)	0.481 (0.125)	0.729 (0.136)	0.720 (0.179)	0.684 (0.191)	
	ARI	0.334 (0.140)	0.348 (0.167)	0.644 (0.190)	0.655 (0.218)	0.610 (0.248)	
	macro-F ₁	0.586 (0.081)	0.629 (0.094)	0.883 (0.076)	0.869 (0.097)	0.835 (0.133)	

The best value in each metric is indicated by bold. The standard deviation is indicated in parentheses. N/A indicates that an algorithm could not build a predictive model.

TABLE 6: Results of the number of leaf nodes in the stationary environment

Type	Dataset	GHNG	GH-EXIN	HFTCA	CAEA	HCAEA
Synthetic	Aggregation	23.2 (1.9)	141.2 (9.4)	108.8 (12.1)	35.5 (4.1)	445.7 (55.2)
	Compound	14.8 (1.8)	136.5 (9.7)	64.7 (5.7)	28.0 (2.8)	33.9 (15.5)
	HardDistribution	14.0 (0.0)	294.7 (40.5)	79.6 (10.4)	30.1 (1.6)	30.1 (1.6)
	Jain	11.9 (1.4)	95.1 (6.9)	50.1 (5.8)	25.4 (3.4)	245.1 (35.2)
	Pathbased	39.3 (3.2)	311.9 (9.4)	43.1 (5.1)	33.2 (4.9)	685.6 (73.9)
Real-world	Breast Cancer	3.0 (0.0)	33.8 (3.6)	54.0 (6.1)	25.7 (3.3)	65.8 (15.0)
	COIL20	65.5 (13.4)	2255.8 (144.8)	34.6 (3.5)	32.4 (2.5)	32.4 (2.5)
	Iris	9.8 (1.5)	86.1 (5.1)	25.9 (5.7)	25.6 (3.9)	218.7 (29.9)
	Isolet	154.7 (4.1)	1226.9 (134.8)	76.1 (14.3)	38.3 (7.2)	400.5 (127.1)
	OptDigits	8.5 (1.5)	72.4 (6.9)	723.9 (19.3)	25.6 (2.6)	168.7 (16.7)
	Seeds	3.6 (1.2)	49.2 (4.6)	45.2 (6.1)	25.4 (2.8)	69.4 (19.6)
	Sonar	3.8 (1.3)	44.7 (8.1)	15.7 (2.3)	23.9 (2.2)	23.9 (2.2)
	TOX171	3.0 (0.0)	31.0 (8.2)	N/A	27.3 (3.2)	27.3 (3.2)
	Wine	3.9 (1.4)	41.6 (4.7)	35.0 (3.5)	21.9 (3.4)	28.4 (8.8)

The standard deviation is indicated in parentheses.
N/A indicates that an algorithm could not build a predictive model.

TABLE 7: Results of training time on CPU in the stationary environment

Type	Dataset	GHNG	GH-EXIN	HFTCA	CAEA	HCAEA
Synthetic	Aggregation	17.078 (1.408)	1.112 (0.093)	16.860 (1.656)	7.736 (0.512)	16.709 (2.077)
	Compound	0.709 (0.070)	2.512 (0.199)	3.306 (0.209)	0.558 (0.064)	0.571 (0.049)
	HardDistribution	0.124 (0.009)	193.311 (13.438)	42.863 (5.481)	1.679 (0.101)	1.703 (0.091)
	Jain	3.012 (0.263)	0.824 (0.192)	2.951 (0.212)	1.624 (0.121)	3.275 (0.248)
	Pathbased	60.086 (4.993)	6.375 (1.199)	2.109 (0.168)	27.056 (2.211)	71.756 (12.270)
Real-world	Breast Cancer	0.241 (0.019)	0.267 (0.023)	0.657 (0.087)	0.221 (0.023)	0.309 (0.028)
	COIL20	1.667 (0.187)	500.936 (116.089)	1.720 (0.100)	11.124 (0.532)	11.120 (0.518)
	Iris	2.761 (0.287)	0.727 (0.066)	0.287 (0.029)	1.489 (0.194)	3.415 (0.322)
	Isolet	34.098 (2.078)	173.905 (66.630)	9.656 (0.731)	38.382 (4.096)	60.154 (7.300)
	OptDigits	2.082 (0.203)	0.804 (0.325)	236.825 (13.707)	1.293 (0.087)	2.374 (0.135)
	Seeds	0.268 (0.034)	0.432 (0.034)	0.273 (0.019)	0.227 (0.018)	0.377 (0.114)
	Sonar	0.030 (0.003)	1.011 (0.104)	0.040 (0.002)	0.055 (0.003)	0.051 (0.002)
	TOX171	0.002 (0.000)	182.100 (29.984)	N/A	0.024 (0.001)	0.021 (0.002)
	Wine	0.105 (0.015)	0.388 (0.037)	0.108 (0.006)	0.103 (0.031)	0.096 (0.008)

The standard deviation is indicated in parentheses.
N/A indicates that an algorithm could not build a predictive model.

a distribution of a dataset. This problem can be solved by increasing the number of training epochs, but this is a major disadvantage in terms of the concept of continuous learning.

GH-EXIN maintains the superior information extraction performance both in the stationary and non-stationary environments. However, GH-EXIN tends to generate a large number of nodes, and the computation speed of GH-EXIN depends on the number of attributes in a dataset. Although GH-EXIN shows superior information extraction performance, the above characteristics become disadvantages when the algorithm tries to handle a large number of high dimensional real-world data.

The common disadvantage of GNG-based algorithms, namely GHNG and GH-EXIN, is that there are a lot of parameters to be specified in advance (see Table 3). Moreover, a value of parameter specified by grid search is significantly different for each dataset (see Table 4). In particular, a sensitivity of parameter in GH-EXIN is very high compared to other algorithms.

Regarding HFTCA, the information extraction performance is similar to GHNG, and inferior to GH-EXIN,

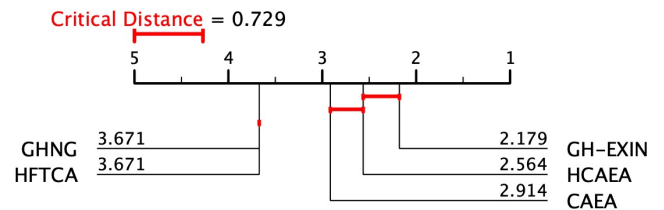


FIGURE 1: Critical difference diagram of classification tasks in the stationary environment.

CAEA, and HCAEA. In addition, a vigilance parameter V , which is a predefined parameter, has to be specified to each layer in advance. If a value of the vigilance parameter V is not properly defined, the algorithm cannot generate the sufficient number of nodes to approximate a distribution of a dataset.

CAEA maintains the better information extraction performance than GHNG and HFTCA without a specification of a large number of parameters both in the stationary and non-stationary environments. One disadvantage of CAEA is that the information extraction performance is significantly

TABLE 8: Results of the classification performance in the non-stationary environment

Type	Dataset	Metric	GHNG	GH-EXIN	HFTCA	CAEA	HCAEA
Synthetic	Aggregation	Accuracy	0.886 (0.043)	0.992 (0.010)	0.478 (0.073)	0.979 (0.026)	0.996 (0.006)
		NMI	0.858 (0.045)	0.986 (0.016)	0.362 (0.043)	0.964 (0.035)	0.992 (0.012)
		ARI	0.795 (0.065)	0.984 (0.019)	0.237 (0.062)	0.956 (0.041)	0.993 (0.012)
		macro-F ₁	0.693 (0.100)	0.984 (0.034)	0.345 (0.072)	0.962 (0.059)	0.993 (0.013)
	Compound	Accuracy	0.781 (0.094)	0.949 (0.035)	0.560 (0.061)	0.936 (0.060)	0.959 (0.035)
		NMI	0.791 (0.086)	0.919 (0.048)	0.430 (0.079)	0.909 (0.070)	0.935 (0.050)
		ARI	0.701 (0.131)	0.905 (0.068)	0.354 (0.093)	0.890 (0.098)	0.922 (0.066)
		macro-F ₁	0.583 (0.142)	0.931 (0.054)	0.344 (0.064)	0.913 (0.089)	0.952 (0.042)
	HardDistribution	Accuracy	0.987 (0.016)	0.991 (0.007)	0.986 (0.010)	0.988 (0.010)	0.984 (0.012)
		NMI	0.951 (0.051)	0.961 (0.030)	0.945 (0.037)	0.951 (0.038)	0.936 (0.043)
		ARI	0.961 (0.049)	0.973 (0.022)	0.959 (0.029)	0.965 (0.028)	0.953 (0.034)
		macro-F ₁	0.987 (0.016)	0.991 (0.007)	0.986 (0.010)	0.988 (0.010)	0.984 (0.012)
	Jain	Accuracy	0.914 (0.056)	1.000 (0.000)	0.851 (0.046)	0.992 (0.026)	1.000 (0.000)
		NMI	0.605 (0.160)	1.000 (0.000)	0.329 (0.127)	0.964 (0.116)	1.000 (0.000)
		ARI	0.673 (0.177)	1.000 (0.000)	0.451 (0.130)	0.969 (0.102)	1.000 (0.000)
		macro-F ₁	0.888 (0.067)	1.000 (0.000)	0.796 (0.061)	0.990 (0.035)	1.000 (0.000)
Pathbased	Accuracy	0.715 (0.109)	0.945 (0.049)	0.528 (0.093)	0.895 (0.081)	0.965 (0.048)	
	NMI	0.510 (0.115)	0.844 (0.120)	0.152 (0.089)	0.765 (0.155)	0.904 (0.119)	
	ARI	0.422 (0.178)	0.837 (0.129)	0.097 (0.095)	0.718 (0.202)	0.895 (0.134)	
	macro-F ₁	0.668 (0.105)	0.943 (0.056)	0.511 (0.086)	0.894 (0.082)	0.965 (0.050)	
Real-world	Breast Cancer	Accuracy	0.897 (0.044)	0.923 (0.031)	0.789 (0.272)	0.911 (0.040)	0.913 (0.041)
		NMI	0.549 (0.139)	0.625 (0.105)	0.420 (0.185)	0.581 (0.144)	0.596 (0.149)
		ARI	0.626 (0.140)	0.710 (0.102)	0.506 (0.208)	0.674 (0.133)	0.680 (0.135)
		macro-F ₁	0.885 (0.048)	0.915 (0.033)	0.779 (0.270)	0.903 (0.044)	0.905 (0.045)
	COIL20	Accuracy	0.416 (0.051)	0.832 (0.054)	0.797 (0.065)	0.646 (0.076)	0.646 (0.076)
		NMI	0.707 (0.042)	0.887 (0.028)	0.891 (0.032)	0.806 (0.037)	0.806 (0.037)
		ARI	0.401 (0.054)	0.756 (0.063)	0.741 (0.078)	0.558 (0.065)	0.558 (0.065)
		macro-F ₁	0.305 (0.048)	0.820 (0.057)	0.766 (0.080)	0.579 (0.085)	0.579 (0.085)
	Iris	Accuracy	0.907 (0.063)	0.933 (0.048)	0.933 (0.061)	0.813 (0.146)	0.913 (0.108)
		NMI	0.840 (0.076)	0.864 (0.085)	0.860 (0.113)	0.787 (0.131)	0.861 (0.121)
		ARI	0.800 (0.107)	0.830 (0.116)	0.841 (0.137)	0.701 (0.196)	0.826 (0.165)
		macro-F ₁	0.868 (0.113)	0.913 (0.074)	0.904 (0.100)	0.759 (0.187)	0.890 (0.137)
	Isolet	Accuracy	0.543 (0.072)	0.779 (0.031)	0.535 (0.031)	0.137 (0.034)	0.137 (0.034)
		NMI	0.691 (0.036)	0.803 (0.021)	0.683 (0.017)	0.347 (0.040)	0.347 (0.040)
		ARI	0.443 (0.056)	0.646 (0.041)	0.421 (0.027)	0.066 (0.022)	0.066 (0.022)
		macro-F ₁	0.504 (0.083)	0.771 (0.033)	0.494 (0.046)	0.053 (0.023)	0.053 (0.023)
	OptDigits	Accuracy	0.899 (0.018)	0.955 (0.009)	0.794 (0.038)	0.683 (0.221)	0.681 (0.219)
		NMI	0.830 (0.025)	0.914 (0.017)	0.701 (0.032)	0.636 (0.171)	0.633 (0.168)
		ARI	0.796 (0.034)	0.904 (0.020)	0.587 (0.076)	0.530 (0.231)	0.526 (0.227)
		macro-F ₁	0.899 (0.018)	0.955 (0.009)	0.802 (0.034)	0.633 (0.270)	0.631 (0.269)
	Seeds	Accuracy	0.867 (0.067)	0.871 (0.054)	0.869 (0.072)	0.826 (0.147)	0.888 (0.070)
		NMI	0.707 (0.119)	0.699 (0.105)	0.692 (0.153)	0.680 (0.154)	0.736 (0.132)
		ARI	0.647 (0.155)	0.657 (0.119)	0.661 (0.180)	0.624 (0.195)	0.699 (0.176)
		macro-F ₁	0.856 (0.082)	0.858 (0.069)	0.851 (0.074)	0.809 (0.148)	0.876 (0.075)
	Sonar	Accuracy	0.486 (0.069)	0.599 (0.091)	0.650 (0.122)	0.671 (0.144)	0.671 (0.144)
		NMI	0.031 (0.042)	0.066 (0.069)	0.137 (0.203)	0.241 (0.140)	0.241 (0.140)
		ARI	0.005 (0.015)	0.043 (0.065)	0.118 (0.209)	0.164 (0.179)	0.164 (0.179)
		macro-F ₁	0.402 (0.098)	0.582 (0.099)	0.631 (0.135)	0.635 (0.157)	0.635 (0.157)
TOX171	Accuracy	0.336 (0.098)	0.406 (0.103)	N/A	0.508 (0.124)	0.508 (0.124)	
	NMI	0.218 (0.120)	0.290 (0.098)	N/A	0.439 (0.155)	0.439 (0.155)	
	ARI	0.061 (0.073)	0.066 (0.087)	N/A	0.223 (0.132)	0.223 (0.132)	
	macro-F ₁	0.247 (0.090)	0.356 (0.122)	N/A	0.409 (0.155)	0.409 (0.155)	
Wine	Accuracy	0.637 (0.096)	0.652 (0.099)	0.866 (0.113)	0.777 (0.148)	0.767 (0.188)	
	NMI	0.460 (0.139)	0.484 (0.111)	0.711 (0.173)	0.604 (0.181)	0.604 (0.223)	
	ARI	0.328 (0.160)	0.345 (0.146)	0.632 (0.212)	0.486 (0.237)	0.502 (0.278)	
	macro-F ₁	0.570 (0.092)	0.624 (0.092)	0.870 (0.114)	0.763 (0.164)	0.752 (0.191)	

The best value in each metric is indicated by bold. The standard deviation is indicated in parentheses. N/A indicates that an algorithm could not build a predictive model.

TABLE 9: Results of the number of leaf nodes in the non-stationary environment

Type	Dataset	GHNG	GH-EXIN	HFTCA	CAEA	HCAEA
Synthetic	Aggregation	23.9 (2.3)	139.1 (8.7)	107.1 (9.9)	74.6 (6.5)	498.0 (75.2)
	Compound	14.5 (1.6)	130.1 (11.3)	63.0 (5.5)	29.9 (4.1)	50.6 (24.0)
	HardDistribution	14.0 (0.0)	292.9 (34.1)	71.7 (14.9)	87.3 (9.3)	87.3 (9.3)
	Jain	11.6 (1.6)	93.4 (7.8)	58.4 (6.6)	39.0 (3.9)	278.6 (32.5)
	Pathbased	39.5 (2.3)	305.6 (11.6)	46.4 (5.1)	66.8 (9.6)	559.9 (130.1)
Real-world	Breast Cancer	3.0 (0.0)	33.6 (3.3)	48.4 (17.4)	27.4 (3.4)	40.4 (4.8)
	COIL20	71.3 (12.4)	1758.5 (238.6)	66.7 (4.8)	39.8 (2.3)	39.8 (2.3)
	Iris	10.1 (1.4)	87.0 (4.5)	25.5 (3.7)	38.8 (4.4)	231.5 (35.2)
	Isolet	155.2 (8.1)	1265.2 (97.7)	56.3 (11.0)	100.8 (51.5)	110.8 (65.3)
	OptDigits	9.4 (1.2)	74.5 (6.0)	1091.4 (13.1)	35.9 (3.5)	191.6 (22.2)
	Seeds	3.5 (1.1)	48.1 (3.9)	43.5 (5.3)	27.9 (3.0)	50.8 (23.6)
	Sonar	3.5 (1.1)	46.7 (5.9)	16.8 (2.6)	23.1 (2.0)	23.1 (2.0)
	TOX171	3.0 (0.0)	33.2 (8.4)	N/A	27.5 (3.6)	27.5 (3.6)
	Wine	3.5 (1.1)	42.8 (3.1)	31.7 (3.3)	24.6 (3.7)	27.4 (4.0)

The standard deviation is indicated in parentheses.
N/A indicates that an algorithm could not build a predictive model.

TABLE 10: Results of training time on CPU in the non-stationary environment

Dataset	GHNG	GH-EXIN	HFTCA	CAEA	HCAEA	
Type	Dataset	GHNG	GH-EXIN	HFTCA	CAEA	HCAEA
Synthetic	Aggregation	43.125 (7.952)	2.097 (0.320)	110.278 (13.641)	64.900 (2.274)	76.470 (6.296)
	Compound	0.759 (0.066)	2.638 (0.206)	3.633 (0.276)	0.817 (0.157)	0.958 (0.241)
	HardDistribution	0.158 (0.021)	330.892 (151.078)	46.797 (8.806)	2.529 (0.229)	2.573 (0.242)
	Jain	3.096 (0.293)	0.918 (0.322)	3.304 (0.237)	4.443 (0.501)	4.470 (0.931)
	Pathbased	63.483 (3.684)	6.247 (0.645)	2.199 (0.172)	36.101 (2.311)	60.177 (7.249)
Real-world	Breast Cancer	0.244 (0.018)	0.276 (0.025)	0.759 (0.268)	0.270 (0.037)	0.301 (0.040)
	COIL20	1.665 (0.134)	379.113 (43.146)	1.992 (0.182)	12.973 (0.422)	13.036 (0.629)
	Iris	2.961 (0.399)	0.784 (0.073)	0.316 (0.036)	2.299 (0.718)	4.003 (0.648)
	Isolet	36.363 (1.707)	119.191 (10.419)	7.894 (0.587)	57.970 (10.203)	60.253 (12.377)
	OptDigits	2.220 (0.182)	0.791 (0.263)	347.531 (15.500)	1.355 (0.294)	2.687 (0.396)
	Seeds	0.273 (0.030)	0.428 (0.039)	0.300 (0.021)	0.257 (0.086)	0.377 (0.162)
	Sonar	0.029 (0.003)	0.964 (0.114)	0.042 (0.002)	0.058 (0.010)	0.056 (0.007)
	TOX171	0.002 (0.000)	204.276 (29.950)	N/A	0.023 (0.002)	0.024 (0.002)
	Wine	0.105 (0.014)	0.383 (0.033)	0.110 (0.013)	0.101 (0.026)	0.104 (0.026)

The standard deviation is indicated in parentheses.
N/A indicates that an algorithm could not build a predictive model.

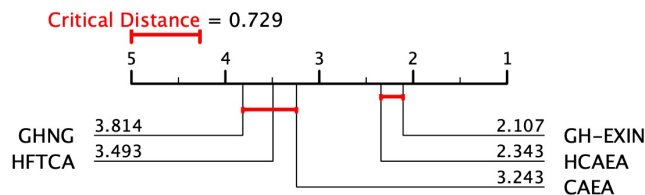


FIGURE 2: Critical difference diagram of classification tasks in the non-stationary environment.

different among the stationary and non-stationary environments. By introducing a hierarchical structure to CAEA, HCAEA successfully solves the disadvantage of CAEA. Furthermore, HCAEA shows the better information extraction performance than CAEA and comparable it to GH-EXIN without a specification of a large number of parameters.

VI. CONCLUSION

This paper proposed an ART-based topological clustering algorithm, called CAEA. CAEA automatically estimates a

similarity threshold, i.e., a vigilance parameter, from a distribution of a dataset. In addition, a divisive hierarchical clustering algorithm capable of continual learning, called HCAEA, is also proposed by applying a hierarchical structure to CAEA. The experimental results showed that the hierarchical structure of HCAEA improves the information extraction ability while solving a disadvantage of CAEA. Moreover, HCAEA has various advantages and the comparative clustering performance compared with recently proposed hierarchical clustering algorithms.

In this paper, we focused only on the avoidance of catastrophic forgetting as a continual learning ability. However, dealing with concept drift, i.e., the concepts of learned information change over time, is also important for maintaining a continual learning ability [38]. Therefore, as a future research topic, we will consider dealing with concept drift in HCAEA in order to extend the functionality of the algorithm.

REFERENCES

- [1] A. Rauber, D. Merkl, and M. Dittenbach, "The growing hierarchical self-organizing map: Exploratory analysis of high-dimensional data," IEEE

- Transactions on Neural Networks, vol. 13, no. 6, pp. 1331–1341, 2002.
- [2] E. J. Palomo and E. López-Rubio, “The growing hierarchical neural gas self-organizing neural network,” *IEEE Transactions on Neural Networks and Learning Systems*, vol. 28, no. 9, pp. 2000–2009, 2016.
 - [3] T. Kohonen, “Self-organized formation of topologically correct feature maps,” *Biological Cybernetics*, vol. 43, no. 1, pp. 59–69, 1982.
 - [4] B. Fritzke, “A growing neural gas network learns topologies,” *Advances in Neural Information Processing Systems*, vol. 7, pp. 625–632, 1995.
 - [5] G. A. Carpenter and S. Grossberg, “The ART of adaptive pattern recognition by a self-organizing neural network,” *Computer*, vol. 21, no. 3, pp. 77–88, 1988.
 - [6] S. Grossberg, “Competitive learning: From interactive activation to adaptive resonance,” *Cognitive Science*, vol. 11, no. 1, pp. 23–63, 1987.
 - [7] G. A. Carpenter, S. Grossberg, and D. B. Rosen, “Fuzzy ART: Fast stable learning and categorization of analog patterns by an adaptive resonance system,” *Neural Networks*, vol. 4, no. 6, pp. 759–771, 1991.
 - [8] B. Vigdor and B. Lerner, “The Bayesian ARTMAP,” *IEEE Transactions on Neural Networks*, vol. 18, no. 6, pp. 1628–1644, 2007.
 - [9] M. Tscherepanow, “TopoART: A topology learning hierarchical ART network,” in *Proceedings of International Conference on Artificial Neural Networks*. Springer, 2010, pp. 157–167.
 - [10] N. Masuyama, C. K. Loo, and F. Dawood, “Kernel Bayesian ART and ARTMAP,” *Neural Networks*, vol. 98, pp. 76–86, 2018.
 - [11] N. Masuyama, C. K. Loo, H. Ishibuchi, N. Kubota, Y. Nojima, and Y. Liu, “Topological clustering via adaptive resonance theory with information theoretic learning,” *IEEE Access*, vol. 7, pp. 76 920–76 936, 2019.
 - [12] N. Masuyama, N. Amako, Y. Nojima, Y. Liu, C. K. Loo, and H. Ishibuchi, “Fast topological adaptive resonance theory based on correntropy induced metric,” in *Proceedings of IEEE Symposium Series on Computational Intelligence*, 2019, pp. 2215–2221.
 - [13] W. Liu, P. P. Pokharel, and J. C. Principe, “Correntropy: Properties and applications in non-Gaussian signal processing,” *IEEE Transactions on Signal Processing*, vol. 55, no. 11, pp. 5286–5298, 2007.
 - [14] Y. Yamada, N. Masuyama, N. Amako, Y. Nojima, C. K. Loo, and H. Ishibuchi, “Divisive hierarchical clustering based on adaptive resonance theory,” in *Proceedings of International Symposium on Community-centric Systems*. IEEE, 2020, pp. 1–6, doi: 10.1109/CcS49175.2020.9231474.
 - [15] G. J. McLachlan, S. X. Lee, and S. I. Rathnayake, “Finite mixture models,” *Annual Review of Statistics and its Application*, vol. 6, pp. 355–378, 2019.
 - [16] S. Lloyd, “Least squares quantization in PCM,” *IEEE Transactions on Information Theory*, vol. 28, no. 2, pp. 129–137, 1982.
 - [17] S. Furoo and O. Hasegawa, “An incremental network for on-line unsupervised classification and topology learning,” *Neural Networks*, vol. 19, no. 1, pp. 90–106, 2006.
 - [18] S. Marsland, J. Shapiro, and U. Nehmzow, “A self-organising network that grows when required,” *Neural Networks*, vol. 15, no. 8, pp. 1041–1058, 2002.
 - [19] G. I. Parisi, J. Tani, C. Weber, and S. Wermter, “Lifelong learning of human actions with deep neural network self-organization,” *Neural Networks*, vol. 96, pp. 137–149, 2017.
 - [20] C. Wiwatcharakoses and D. Berrar, “SOINN+, a self-organizing incremental neural network for unsupervised learning from noisy data streams,” *Expert Systems with Applications*, vol. 143, p. 113069, 2020.
 - [21] —, “A self-organizing incremental neural network for continual supervised learning,” *Expert Systems with Applications*, vol. 185, p. 115662, 2021.
 - [22] S. C. Tan, J. Watada, Z. Ibrahim, and M. Khalid, “Evolutionary fuzzy ARTMAP neural networks for classification of semiconductor defects,” *IEEE Transactions on Neural Networks and Learning Systems*, vol. 26, no. 5, pp. 933–950, 2014.
 - [23] A. L. Matias and A. R. R. Neto, “OnARTMAP: A fuzzy ARTMAP-based architecture,” *Neural Networks*, vol. 98, pp. 236–250, 2018.
 - [24] A. L. Matias, A. R. R. Neto, C. L. C. Mattos, and J. P. P. Gomes, “A novel fuzzy ARTMAP with area of influence,” *Neurocomputing*, vol. 432, pp. 80–90, 2021.
 - [25] L. Wang, H. Zhu, J. Meng, and W. He, “Incremental local distribution-based clustering using Bayesian adaptive resonance theory,” *IEEE Transactions on Neural Networks and Learning Systems*, vol. 30, no. 11, pp. 3496–3504, 2019.
 - [26] L. E. B. da Silva, I. Elnabarawy, and D. C. Wunsch II, “Distributed dual vigilance fuzzy adaptive resonance theory learns online, retrieves arbitrarily-shaped clusters, and mitigates order dependence,” *Neural Networks*, vol. 121, pp. 208–228, 2020.
 - [27] A. Saxena, M. Prasad, A. Gupta, N. Bharill, O. P. Patel, A. Tiwari, M. J. Er, W. Ding, and C.-T. Lin, “A review of clustering techniques and developments,” *Neurocomputing*, vol. 267, pp. 664–681, 2017.
 - [28] Y. Wang and B. Moseley, “An objective for hierarchical clustering in euclidean space and its connection to bisecting k -means,” in *Proceedings of AAAI Conference on Artificial Intelligence*, vol. 34, no. 4, 2020, pp. 6307–6314.
 - [29] D. Boley, “Principal direction divisive partitioning,” *Data Mining and Knowledge Discovery*, vol. 2, no. 4, pp. 325–344, 1998.
 - [30] G. Cirrincione, G. Ciravegna, P. Barbiero, V. Randazzo, and E. Pasero, “The GH-EXIN neural network for hierarchical clustering,” *Neural Networks*, vol. 121, pp. 57–73, 2020.
 - [31] D. J. Henderson and C. F. Parmeter, “Normal reference bandwidths for the general order, multivariate kernel density derivative estimator,” *Statistics & Probability Letters*, vol. 82, no. 12, pp. 2198–2205, 2012.
 - [32] P. Fränti and S. Sieranoja, “K-means properties on six clustering benchmark datasets,” *Applied Intelligence*, vol. 48, no. 12, pp. 4743–4759, 2018.
 - [33] W. Liu, Z. Wang, X. Liu, N. Zeng, Y. Liu, and F. E. Alsaadi, “A survey of deep neural network architectures and their applications,” *Neurocomputing*, vol. 234, pp. 11–26, 2017.
 - [34] D. Dua and C. Graff, “UCI machine learning repository,” University of California, Irvine, School of Information and Computer Sciences, 2019. [Online]. Available: <http://archive.ics.uci.edu/ml>
 - [35] A. Strehl and J. Ghosh, “Cluster ensembles—A knowledge reuse framework for combining multiple partitions,” *Journal of Machine Learning Research*, vol. 3, no. Dec, pp. 583–617, 2002.
 - [36] L. Hubert and P. Arabie, “Comparing partitions,” *Journal of Classification*, vol. 2, no. 1, pp. 193–218, 1985.
 - [37] J. Demšar, “Statistical comparisons of classifiers over multiple data sets,” *Journal of Machine Learning Research*, vol. 7, no. 1, pp. 1–30, 2006.
 - [38] J. Lu, A. Liu, F. Dong, F. Gu, J. Gama, and G. Zhang, “Learning under concept drift: A review,” *IEEE Transactions on Knowledge and Data Engineering*, vol. 31, no. 12, pp. 2346–2363, 2018.



Japan.

His current research interests include clustering, data mining, and continual learning.



NARITO AMAKO received the B.S degree in Computer Science from Osaka Prefecture University, Japan in 2020. He is now a master course student in Department of Computer Science and Intelligent Systems, Osaka Prefecture University. His research interests include data mining and machine learning.



YUNA YAMADA received the B.S degree in Computer Science from Osaka Prefecture University, Japan in 2021. She is now a master course student in Department of Computer Science and Intelligent Systems, Osaka Prefecture University. Her research interests include data mining and machine learning.



YUSUKE NOJIMA received the B.S. and M.S. Degrees in mechanical engineering from Osaka Institute of Technology, Osaka, Japan, in 1999 and 2001, respectively, and the Ph.D. degree in system function science from Kobe University, Hyogo, Japan, in 2004.

Since 2004, he has been with Osaka Prefecture University, Osaka, Japan, where he is currently a Professor in Department of Computer Science and Intelligent Systems.

His research interests include evolutionary fuzzy systems, evolutionary multiobjective optimization, and parallel distributed data mining. He was a guest editor for several special issues in international journals. He was a task force chair on Evolutionary Fuzzy Systems in Fuzzy Systems Technical Committee of IEEE Computational Intelligence Society. He was an associate editor of IEEE Computational Intelligence Magazine (2014-2019).



HISAO ISHIBUCHI (M'93–SM'10–F'14) received the B.S. and M.S. degrees in precision mechanics from Kyoto University, Kyoto, Japan, in 1985 and 1987, respectively, and the Ph.D. degree in computer science from Osaka Prefecture University, Sakai, Osaka, Japan, in 1992.

Since 1987, he has been with Osaka Prefecture University for 30 years. He is currently a Chair Professor with the Department of Computer Science and Engineering, Southern University of

Science Technology, Shenzhen, China. His current research interests include fuzzy rule-based classifiers, evolutionary multiobjective optimization, many-objective optimization, and memetic algorithms.

Dr. Ishibuchi was the IEEE Computational Intelligence Society (CIS) VicePresident for Technical Activities from 2010 to 2013. He was an IEEE CIS AdCom Member from 2014 to 2019, an IEEE CIS Distinguished Lecturer from 2015 to 2017, and an Editor-in-Chief of the IEEE Computational Intelligence Magazine from 2014 to 2019. He is also an Associate Editor of the IEEE TRANSACTIONS ON EVOLUTIONARY COMPUTATION, the IEEE TRANSACTIONS ON CYBERNETICS, and the IEEE ACCESS.